Emergence and role of dipolar dislocation patterns in discrete and continuum formulations of plasticity

Péter Dusán Ispánovity, Stefanos Papanikolaou, and István Groma

Phys. Rev. B **101**, 024105 — Published 10 January 2020

DOI: 10.1103/PhysRevB.101.024105

The Emergence and Role of Dipolar Dislocation Patterns in Discrete and Continuum Formulations of Plasticity

Péter Dusán Ispánovity,[1,*] Stefanos Papanikolaou,[2,3,4] and István Groma[1]

[1] *Department of Materials Physics, Eötvös University, Pázmány Péter sétány 1/a, H-1117 Budapest, Hungary*
[2] *Department of Mechanical Engineering, The West Virginia University*
[3] *Department of Physics, The West Virginia University*
[4] *Department of Mechanical Engineering, The Johns Hopkins University, Baltimore, MD 21218*

(Dated: December 5, 2019)

The plasticity transition, at the yield strength of a crystal, typically signifies the tendency of dislocation defects towards relatively unrestricted motion. An isolated dislocation moves in the slip plane with velocity proportional to the shear stress, while dislocation ensembles move towards satisfying emergent collective elastoplastic modes through the long range interactions. Collective dislocation motions are discussed in terms of the elusively defined *backstress*. In this paper, we present a stochastic continuum model that is based on a two-dimensional continuum dislocation dynamics theory that clarifies the role of backstress and demonstrates a precise agreement with the collective behavior of its discrete counterpart, as a function of applied load and with only three essential free parameters. The main ingredients of the continuum theory is the evolution equations of statistically stored and geometrically necessary dislocation densities, which are driven by the long-range internal stress, a stochastic yield stress and, finally, two local "diffusion" like terms. The agreement is shown primarily in terms of the patterning characteristics that include the formation of dipolar dislocation walls.

Crystals mainly deform through the motion of dislocations [1], extended line-like defects in the crystal lattice. This sole fact can provide key explanations for the magnitude and character of uniaxial and shear strength, as well as the plastic crystalline behavior. However, the complex spatio-temporal dynamics of dislocations is elusive: It has long been known that many aspects of the stress-strain response of deformed metals are associated to collective and emergent dislocation patterning that cannot be predicted by single-dislocation features, e.g., dense dipolar wall (DDW) formation and corresponding dislocation cell walls (see for example, Refs. [2–8]). Also, failure due to mechanical fatigue is preceded by the formation of complex dislocation patterns that have been labeled as "vein structures", typically observed after multiple thousands of fatigue cycles [9–13]. Dislocation patterning is, therefore, not only interesting in relation to analogous phenomena in statistical mechanics [14], but also it correlates with the vital technological interest of characterizing and predicting the lifetime of mechanical components [9].

Although during the past five decades several attempts have been proposed to model pattern formation [15–20] most of them are based on purely phenomenological arguments, so they are not derived from the properties of individual dislocations. Very recently, however, models based on statistical physics considerations have been derived establishing a direct link between a micro and mesoscale descriptions of the collective motion of dislocations [21–26]. Yet, neither the dynamical or energetic origin of DDWs (or that of the vein structures or other specific dislocation patterns) was clarified, nor their relation to *back-stress* terms (induced by dislocation correlations schematically shown in Fig. 1) appearing in continuum dislocation dynamics. These latter dislocation force components are typically associated with the Bauschinger effect (the asymmetry of deformation upon reversed loading) and represent key ingredients of kinematic hardening theories [1, 27, 28]. In dislocation dynamics and strain-gradient plasticity theories [29], such terms involve nonlinear derivatives of the local dislocation density, however their precise form has been elusive [21, 30, 31].

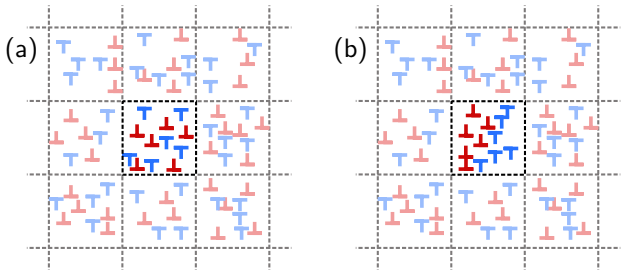

FIG. 1. A gradient in the geometrically necessary dislocation density is one form of spatial correlations that may affect local strength (through the back-stress τ_b) and lead to different yielding thresholds for panels (a) and (b). Configuration of panel (b) is stronger (weaker) if $D < 0$ ($D > 0$). The dashed lines denote spatial discretization which is necessary to define continuous densities.

In this paper, we develop further the deterministic approach proposed by Groma *et al.* [25] that is able to display the spontaneous formation of dislocation walls through a dynamical transition [14], and can be used to establish basic constitutive rules for continuum dislocation plasticity theories. The key ingredients are: a

* ispanovity@metal.elte.hu

TABLE I. Summary of the units of dimensionless quantities.

Quantity	Unit
Distance (x)	$\rho_0^{-1/2}$
Stress (τ)	$Gb\rho_0^{1/2}$
Plastic strain (γ)	$b\rho_0^{1/2}$
Time (t)	$MGb^2\rho_0$
Dislocation density (ρ, κ)	ρ_0

particular form of dislocation backstress, a "diffusion" like stress term proportional to the gradient of the statistically stored dislocation density, and the yield stress being proportional to the square root of the statistically stored dislocation density (Taylor hardening law). Each term arises from a consistent coarse-graining procedure and contains dimensionless prefactors. Here we show that although patterning is a general feature of the original model [25, 32], realistic DDW formation observed in lower scale discrete dislocation dynamics (DDD) simulations [33] only occurs when the yield stress is replaced by a local random variable that makes the model stochastic. Such random terms were previously used in general plasticity models for crystal [34] and amorphous [35] plasticity and its precise form for 2D dislocation plasticity has been determined recently from DDD simulations [36]. Our results, therefore, shed new light on the role of the backstress as well as the stochastic local yield threshold in dislocation patterning of bulk single crystals, and provide a successful multi-scale description of the dynamics in single-slip edge dislocation systems.

The emergence of dislocation patterns has been investigated numerically using multiple approaches, including two-dimensional(2D) [33, 37–44], three-dimensional (3D) DDD [45, 46], as well as continuum dislocation dynamics (CDD) [47–50]. Realistic 3D-DDD have been too expensive and remain below 1% strain in bulk conditions, while CDD has not yet captured local entanglement and backstress interactions that are expected to play critical role in patterning [51, 52]. In contrast, 2D-DDD methods not only are numerically tractable at large strains, but also a rigorous coarse graining procedure has been developed for the special case of edge dislocations in single slip [21, 23, 25]. In this paper, we will investigate the continuum description of patterns in this case.

We consider a configuration of straight parallel edge dislocations, lying along the z axis with their Burgers vectors pointing in the x direction. We assume to track the motion of dislocations on the $z = 0$ plane. To emulate an infinite crystalline medium, periodic boundary conditions (PBC) are applied at the borders of the square shaped simulation area of size $L \times L$. The Burgers vector can be written as $\boldsymbol{b}_i = s_i\boldsymbol{b}$, where $\boldsymbol{b} = (b, 0)$, $s_i = \pm 1$, and $1 \leq i \leq N$, with N being the total number of dislocations. To mimic easy glide a linear relationship is assumed between the projection of the Peach-Koehler force to the glide plane (denoted by F hereafter) and the dislocation velocity in the glide direction v as $v = MF$, where M is the dislocation mobility [53]. Throughout of this paper dimensionless units summarized in Table I are used where $\rho_0 = N/L^2$ is the average total dislocation density and $G = \mu/[2\pi(1-\nu)]$ is an elastic constant (where μ and ν is the shear modulus and Poisson's number, respectively). Using these units the equation of motion for the ith discrete dislocation ($0 \geq i \geq N$) reads as

$$\dot{x}_i(t) = s_i \left[\tau_{\text{ext}} + \sum_{j=1, j\neq i}^{N} s_j \tau_{\text{ind}}(\boldsymbol{r}_i - \boldsymbol{r}_j) \right] ; \; \dot{y}_i(t) = 0, \tag{1}$$

where τ_{ind} denotes the shear stress field of an individual dislocation (see, e.g., [38]). For further details on our 2D-DDD simulations and the exact formula for τ_{ind} see the Supplemental Material [54] (see, also, references [21, 23, 25, 34, 36, 38, 55–57] therein).

The typical evolution of a dislocation configuration can be seen in the left column of Fig. 2. At zero applied shear stress τ_{ext} no clear pattern can be observed even though there are specific local (low energy) configurations: Opposite sign dislocations organize into short dipoles whereas those of identical sign form short vertical walls. As τ_{ext} increases, dislocation patterns become increasingly heterogeneous with predominant long dense vertical walls [33]. These DDWs are induced by the external shear stress and represent the most stable configuration that can be formed in this 2D system. Recently, it has been shown that orientation of the slip system with respect to the simulation box strongly influences the correlation properties of the dislocation network at large strains [58]. This type of boundary condition sensitivity is common to patterning instabilities in condensed matter systems with long-range interactions [59]. In all such systems, the local interaction that causes the instability is believed to be independent of the particular boundary condition to be investigated. Thus, in the present system, the emergent local order is not expected to be affected by boundary conditions at small strains.

To characterize the pattern evolution in a quantitative manner the two-point spatial correlation functions are computed at different strain levels. These functions are defined as

$$d_{++}(\boldsymbol{r}) = \left\langle \frac{\rho_{++}(\boldsymbol{r}', \boldsymbol{r}' + \boldsymbol{r})}{\rho_0^2} - 1 \right\rangle_{\boldsymbol{r}'}, \tag{2}$$

where $\rho_{++}(\boldsymbol{r}', \boldsymbol{r})$ denotes the two-point density of a + sign dislocation at $\boldsymbol{r}'$ and a + sign dislocation at $\boldsymbol{r}' + \boldsymbol{r}$ [60]. In the definition the averaging with respect to $\boldsymbol{r}'$ is introduced since the system due to the PBC is homogeneous, so, $\rho_{++}(\boldsymbol{r}_1, \boldsymbol{r}_2)$ can only depend on the relative coordinate $\boldsymbol{r}_2 - \boldsymbol{r}_1$. The correlation function for the opposite sign dislocations d_{+-} is defined accordingly. The numerically obtained correlation functions and their evolution with increasing strain can be seen in the center and right column of Fig. 2. These functions were averaged over 200 individual realizations, so, they represent the

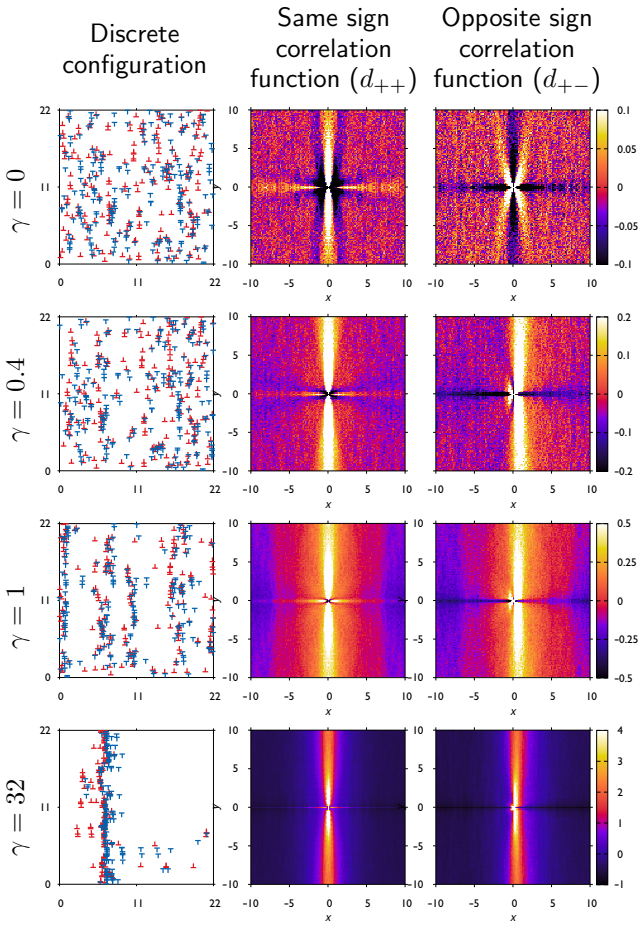

FIG. 2. Dislocation pattern evolution in DDD simulations. Left column: Dislocation configurations obtained at different strain γ values. Middle and right columns: Same sign and opposite sign spatial correlation functions (d_{++} and d_{+-}, respectively) of discrete dislocations.

average patterning behavior of the DDD system. At zero strain the microstructure is dominated by vertical walls of same sign dislocations and short dipoles of opposite sign dislocations having a 45° angle with the horizontal glide plane. The d_{++} function has a slow $|y|^{-1.5}$ type power-law decay along the y axis, signalling a broad distribution of the wall lengths [22]. With increasing strain

(i) the walls get longer and denser (see the change in the magnitude of the correlation function d_{++}) and

(ii) the function d_{+-} becomes asymmetric due to the polarization of the microstructure, that is, the $-$ sign dislocations tend to be positioned to the right with respect to the $+$ sign dislocations. In addition, with accumulating strain the d_{+-} function extends in the vertical direction similarly to the d_{++} signalling the build-up of the DDWs seen in the left column of Fig. 2.

In order to identify the precise continuum form of the DDW instability in the 2D-DDD simulations, we consider the theory that has been directly derived from the equations of motion (see SI) using a rigorous coarse graining procedure [25], and is based on the continuous density fields $\rho_\pm(\boldsymbol{r},t)$ of dislocations with identical ($+$ or $-$) sign, and the corresponding total dislocation density $\rho = \rho_+ + \rho_-$ and geometrically necessary dislocation (GND) density $\kappa = \rho_+ - \rho_-$. The recently revisited form of the evolution equations with the dimensionless variables of Table I read as follows:

$$\partial_t \rho_+ = -\partial_x \left\{ \rho_+ \left[\tau_{\rm ext} + \tau_{\rm sc} + \tau_b - 2\frac{\rho_-}{\rho}\tau_f + \tau_d \right] \right\}, \quad (3)$$

$$\partial_t \rho_- = +\partial_x \left\{ \rho_- \left[\tau_{\rm ext} + \tau_{\rm sc} + \tau_b - 2\frac{\rho_+}{\rho}\tau_f - \tau_d \right] \right\}, \quad (4)$$

where

$$\tau_{\rm sc}(\boldsymbol{r},t) = \int \tau_{\rm ind}(\boldsymbol{r}-\boldsymbol{r}')\kappa(\boldsymbol{r}',t)\mathrm{d}^2 r' \quad (5)$$

is the long-range (or "self-consistent") stress field of GNDs which together with the external field $\tau_{\rm ext}$ represents the experimentally measurable average shear stress in a small volume around $\boldsymbol{r}$. This is complemented by the gradient stress components

$$\tau_b(\boldsymbol{r},t) = -\frac{D}{\rho}\partial_x \kappa(\boldsymbol{r},t) \ \text{ and } \ \tau_d(\boldsymbol{r},t) = -\frac{A}{\rho}\partial_x \rho(\boldsymbol{r},t). \quad (6)$$

and friction stress τ_f that is as big as necessary to prevent dislocation flow and it cannot be larger than the yield stress $\alpha\rho^{1/2}$. In the equations above, α, D and A are dimensionless constants: α is the dimensionless parameter of the Taylor hardening law whereas A and D are specific moments of the dislocation interaction stress $\tau_{\rm ind}$ and the two-point correlation functions [21]. Note, that, as described above, material-dependent Burgers vector, elastic constants and dislocation mobility were absorbed into time and stress scales, so all quantities in the above equations are dimensionless. For the dimensional versions, see [25].

The origin of the friction stress τ_f and local gradient terms τ_b (back-stress) and τ_d (diffusion stress) is clear from the formal derivation of the theory [25]: They stem from the fact that dislocations are not positioned randomly but are spatially correlated, a fact that has been already postulated by Wilkens based on energetic considerations [61], also demonstrated in numerical simulations [60] and in Fig. 2. Dislocation patterns themselves are also a manifestation of these correlations (see, for example, Fig. 1 for a schematic). As of the physical meaning of these terms, friction stress, and so the yield stress, is the result of the small-scale correlated substructures (most importantly, dislocation dipoles in the 2D system being studied) that may be stable against external load. Indeed, in Eqs. (3,4) τ_f is multiplied by $\rho_\pm/\rho$ expressing that dislocations can only be withheld by dislocations of opposite sign. Interpretation of gradient terms are more subtle: In the flowing regime they can be envisaged as a correction to the yield stress. In particular, due to

the back-stress term local strength may depend on the gradient of the GND density as depicted in the sketch of Figure 1. According to the sign of parameter D, the strength of the local volume in Fig. 1(b) may be larger (for $D < 0$) or smaller (for $D > 0$) than that of Fig. 1(a). Similar explanation can be given for the diffusion stress τ_d.

The importance of our formulation becomes transparent when one aims at building a multiscale connection and understanding of traditional plasticity theories of constitutive formulations of backstress fields to discrete dislocation formulations [1]. In traditional formulations, the most common approach involves the modeling of backstress χ in a particular slip system, as a correction to the shear stress τ, that displays a typical evolution equation with direct hardening and dynamic recovery coefficients respectively (see for example Ref. [62]):

$$\dot{\chi} = c\dot{\gamma} - d\chi|\dot{\gamma}| \tag{7}$$

where $\gamma, \dot{\gamma}$ are the shear strain and strain rates in the slip system. This equation has a natural, intuitive and experimentally verifiable explanation in terms of polycrystalline, grain-boundary dominated plasticity, since it is transparent that dislocations that "cross" grain-boundaries should face an opposite-signed, discontinuous resistance when loaded in the opposite direction. However, in dislocation ensembles, such explanations were elusive and vague, especially since continuum dislocation density theories desire continuous, analytic terms if not required otherwise. Nevertheless, in the single-slip theory we have developed, it is transparent how the d-term in Eq. (7) emerges, without the particular need of non-analytic mathematical terms. As shown in Fig. 3, the response of a continuum dipolar wall in our theory contains all the ingredients that were constitutively assumed in traditional multiscale formulations: If a positive-signed dislocation moves across the wall, it would have an opposite-signed resistance if moved in opposite directions.

The numerical implementation is based on the phase-field functional:

$$P[\rho, \kappa] = E_{\rm el} + \int \left[A\rho \ln\left(\frac{\rho}{\rho_0}\right) + \frac{D}{2}\frac{\kappa^2}{\rho} \right] {\rm d}^2 r, \tag{8}$$

where $E_{\rm el}$ is the mean-field stored elastic energy of the system (measured in units of Gb^2) that includes information about the self-consistent and external stress fields (see its exact form in the SM) [25], and ρ_0 is a constant that does not appear in the evolution equations. It was shown before that Eqs. (3,4) can be derived from Eq. (8) assuming that $|\kappa| \ll \rho$ and that P can only decrease during the evolution of the system [25]. In the present implementation, densities are discretized on a regular grid of cell size a, and the yield stress (that is, the maximum of the friction stress τ_f) is replaced by a local stochastic variable (representing the fluctuations of the underlying dislocation microstructure at every cell). For the

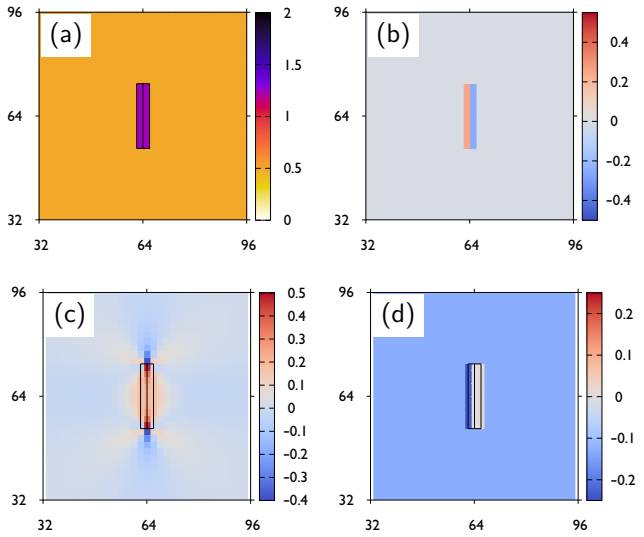

FIG. 3. Stress fields in a model of a dipolar wall in the SCDD. (a,b): Total and GND densities of a dipolar wall placed in a constant dislocation density background. (c) Self-consistent field $\tau_{\rm sc}$ of the dipolar wall. (d) Gradient stresses ($\tau_b + \tau_d$) acting on a positive sign ($s = 1$) dislocation. Notice the development of a back-stress on the left side of the dipolar wall. The model parameters used are the same as in Fig. 4.

distribution of the yield stress, in accordance with recent DDD results, a Weibull distribution is used with shape parameter 1.4 and the scale parameter is defined through $\langle \tau_f \rangle = \alpha\sqrt{\rho}$ (see details in the SM) [36]. We apply extremal dynamics: At every timestep, dislocation activity takes place at the site where decrease in P is the largest and this consists of a quantum of dislocation flux $\Delta\rho = a^{-2}$ (of either positive or negative dislocations) flowing through the cell boundary. If no such cell exists, external stress $\tau_{\rm ext}$ is increased until one cell is triggered. After each triggering, a new random yield stress from the same Weibull distribution is assigned to the given cell. Further details of the implementation are summarized in the Supplemental Material [54]. In the rest of this paper this model is referred to as stochastic continuum dislocation dynamics (SCDD).

The continuum theory does not yield exact values for the parameters α, D, and A; one must, therefore, consider them as fitting parameters. The results of DDD simulations summarized above, however, give insight on possible values. As seen in Fig. 2 the strongest possible dislocation configuration is the dipolar wall structure. According to Fig. 1 this might imply the necessity of the back-stress term τ_b and that $D < 0$. However, according to the linear stability analysis of Eqs. (3,4), in the absence of stochastic terms, which is discussed in Ref. [25], one may conclude that if $D = A = 0$ or either D or A is negative, then all perturbations are unstable, and the fastest growing perturbation is seemingly

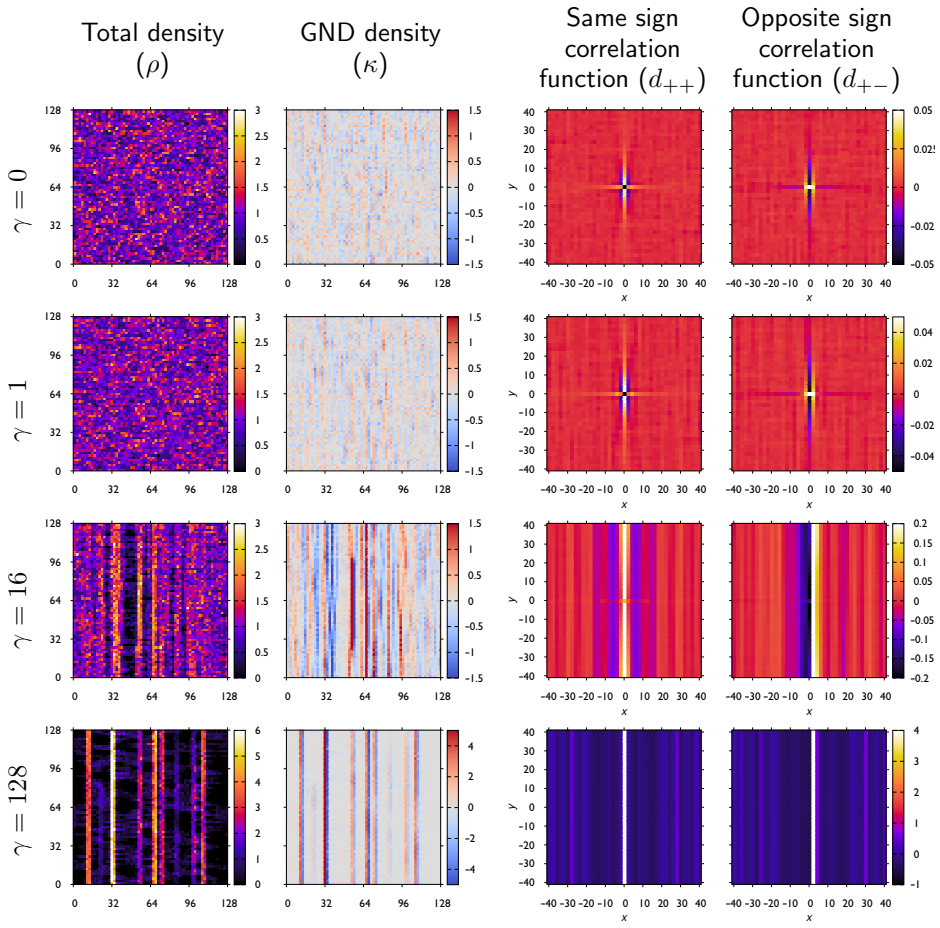

FIG. 4. Dislocation pattern evolution in SCDD simulations with $D = A = 0.25$, $\alpha = 1.0$ and $a = 2$. Left two columns: Total and GND density maps obtained at different strain γ values. Right two columns: Same sign and opposite sign spatial correlation functions (d_{++} and d_{+-}, respectively) of dislocation densities.

the largest possible wave-vector $k_x = 2\pi/|b|$ where $|b|$ is the minimum-possible Burgers vector magnitude. This implies that in such cases the wavelength of the instability approaches the lattice scale, and one would expect a dislocation pattern where positive/negative dislocation walls arrange in a $+-+-$ type instability. In the following, that is exactly what we observe. Moreover, if $A > 0$ and $D > 0$, resulting that the phase field functional given by Eq. (8) is convex, then the linear stability analysis of Ref. [25] concludes that there is an emergent wavelength selection for a periodic pattern that should appear. However, in the presence of quenched stochastic terms, such as the ones considered both in the presented DDD and SCDD models, it is expected that such instabilities would be suppressed by the quenched disorder, which typically takes the form of a stochastic yield stress term. The inclusion of a stochastic yield stress term (such as the one in this work) is critical to suppress non-linear dynamical instabilities that are tied to the particular deterministic dynamical equations and thus, non-generic, and probably this difference may explain particularly different conclusions of our work compared to prior efforts on analogous questions [32].

In accordance with our 2D-DDD simulations, at $t = 0$ a random pattern of ρ_+ and ρ_- is assumed, and initially a relaxation step is performed at $\tau_{\text{ext}} = 0$. Then, the external stress τ_{ext} is quasi-statically increased. The two left columns of Fig. 4 depict this evolution in terms of the total and GND densities (ρ and κ, respectively) for a given parameter set ($D = 0.25$, $A = 0.25$, $\alpha = 1.0$, $a = 2$). Analogous behavior is obtained between DDD and SCDD in the evolution of both total and GND profiles: short vertical DDWs form in the initial phases of deformation which then merge and extend in the vertical direction upon increasing strain. To descibe the patterns in more detail, the correlation functions d_{++} and d_{+-} were also calculated and can be seen in the right two columns of Fig. 4. Although fine details of the correlation functions cannot be reproduced with a continuum method defined on a coarse mesh, the evolution of these functions is remarkably similar to the DDD case (seen in Fig. 2), however, pattern development is somewhat delayed in the SCDD (also note the difference in the spatial scale between DDD and SCDD results). In particular, at strain $\gamma = 0$ the configuration consists of short vertical walls of same sign dislocations and short dislocation

dipoles of opposite sign having an angle of 45 degrees with the x axis. As the stress and strain increases the vertical walls become more extended and strong asymmetry develops in the d_{+-} correlation function signaling the presence of DDWs. To quantitatively compare the polarization due to the asymmetry in d_{+-} between DDD and SCDD we consider the spatial average of d_{+-} along the vertical direction as

$$C_{+-}(x) = (1/L) \int d_{+-}(x, y) \mathrm{d}y \tag{9}$$

which measures the polarization of individual configurations. Indeed Fig. 5 shows that a strong asymmetry emerges upon plastic deformation for both models. In addition, a quick, exponential decay follows the peak in the $x > 0$ domain, with a characteristic distance of approx. 5 average dislocation spacings. This length scale can be identified with the characteristic width of the DDWs. We identify this asymmetry as the most basic origin of the Bauschinger effect [63] as it will be discussed below.

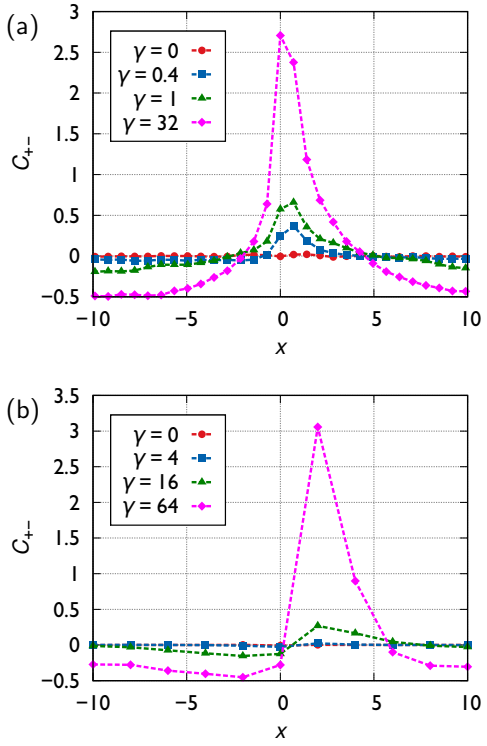

FIG. 5. Correlation functions averaged along the DDW direction C_{+-} for the two applied models: (a) DDD and (b) SCDD. Notice the asymmetry developing upon increasing strain. The simulation parameters are the same as in Figs. 3 and 4.

We now address the role of SCDD parameters in the patterning instability. Figure 6 plots the dependence of typical patterns and the corresponding correlation functions on the coefficients of the gradient terms D and A and the average strength of the yield threshold α. As seen, in the absence of gradient terms ($D = A = 0$) the $+-+-$-type instability discussed above can be clearly observed (second row). This behavior is, in agreement with the theory, induced by the friction stress term τ_f and is at odds with the patterns of DDD and demonstrates the necessity of the inclusion of gradient terms. The third row of Fig. 6 shows the effect of $D < 0$: the increased strength of the GND gradient depicted in Fig. 1 leads to even stronger $+-+-$ instability, again in agreement with the linear stability analysis of Ref. [25]. As of the role of the other parameters, we first recall that τ_d is a diffusive term in the total dislocation density ρ, so increasing the value of A leads to smoothening of the dislocation patterns (see the 4th row of Fig. 6) while $A < 0$ would lead to anti-diffusion and the immediate blow-up of the pattern (not shown). The effect of decreased yield strength is seen in the last row of Fig. 6: one observes weaker patterns and polarization and the increase of α would lead to the strengthening of the $+-+-$ instability. To summarize, it is evident that in order to obtain realistic patterns $D > 0$ and $A > 0$ is required and both too large and too small values of α should be avoided. A more detailed analysis will be published elsewhere.

It is instructive to compare the continuum plasticity theory with general elastoplastic constitutive models and in particular, with those of kinematic hardening [1]. The backstress term appearing therein has the phenomenological role of modeling the Bauschinger effect observed at reversed loading with the appropriate translation of the yield surface. In this paper, we showed that there is an explicit correspondence: since τ_b in Eqs. (3,4) can also be considered as an asymmetric correction to τ_f, and using the identity $\partial_t \kappa(\boldsymbol{r}, t) = -\partial_x \dot{\gamma}(\boldsymbol{r}, t)$, with the GND density connected to the shear component $\dot{\gamma}$ of the plastic strain rate, one arrives at $\dot{\tau}_b = (D/\rho)\partial_x^2 \dot{\gamma}$ that is analogous to the phenomenological rate equation of Melan and Prager ($\dot{\tau}_b \propto \dot{\gamma}$) [64, 65] (the appearance of the second derivative reflects the strain-gradient origin of the Bauschinger effect and the backstress in microscopically derived continuum theories of dislocation behavior). The simulations presented above, therefore, emphasize the microscopic origin of the backstress: The asymmetry of the yield surface in kinematic hardening is the result of the bulid-up of asymmetric dislocation sub-structures (polarized walls in the present set-up). Furthermore, backstress terms are also used in gradient plasticity theories to account for the short-range interactions in pile-ups close to grain boundaries [66]. Such terms exhibit the same form as Eq. (6) also with a positive dimensionless prefactor.

In the case of SCDD the picture that emerges is as follows: the DDWs formed during plastic deformation are in fact two GND pile-ups piling up against each other. The $+-$ instability at the center is due to the yield stress which also provides the great strength of such structures. However, backstress terms are also required to suppress the $+-+-$ instability discussed in the paper and to provide a length-scale for the pile-up widths.

In summary, SCDD does not only provide precise description of its microscopic DDD counterpart, thus rep-

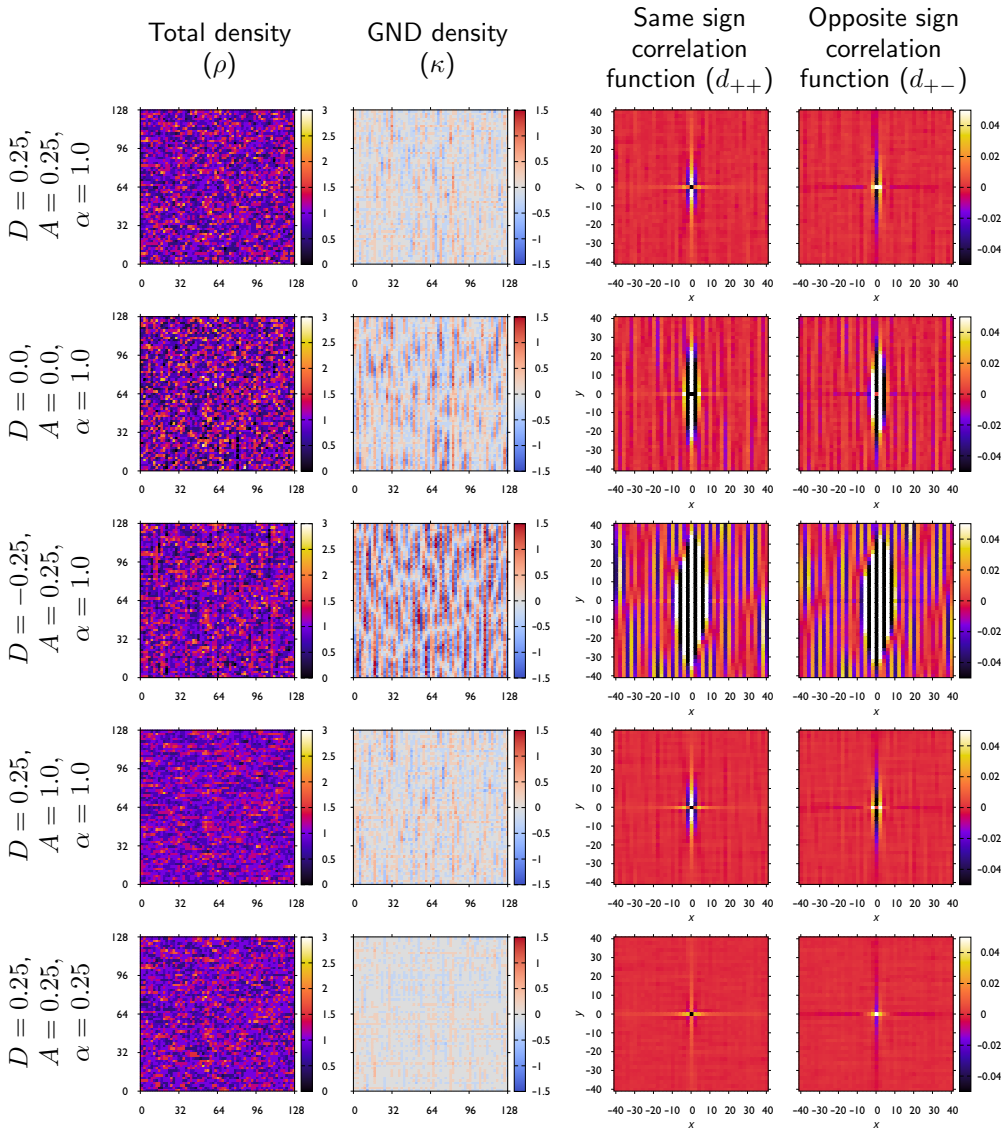

FIG. 6. Dislocation pattern evolution in SCDD simulations for different parameters at $\gamma = 1$ and $a = 2$. Left two columns: Total and GND density maps obtained at different strain γ values. Right two columns: Same sign and opposite sign spatial correlation functions (d_{++} and d_{+-}, respectively) of dislocation densities.

resenting a successful multi-scale step, but it also synthesizes previous theoretical approaches of dislocation pattern formation, kinematic hardening, and strain gradient plasticity in a simple 2D setting. By identifying the physical interpretation and key role of the strain gradient terms our results may serve as a starting point for more complex 3D implementations.

We thank Michael Zaiser for fruitful discussions. This work has been supported by the National Research, Development and Innovation Office of Hungary (PDI and IG, project Nos. NKFIH-K-119561 and NKFIH-KH-125380), the Czech Science Foundation (PDI, project No. 15-10821S) and by the U.S. Department of Energy, Office of Sciences, Basic Energy Sciences, DE-SC0014109 (SP). This work was completed in the ELTE Institutional Excellence Program (1783-3/2018/FEKUTSRAT) supported by the Hungarian Ministry of Human Capacities. PDI is also supported by the ÚNKP-18-4 New National Excellence Program of the Hungarian Ministry of Human Capacities and by the János Bolyai Scholarship of the Hungarian Academy of Sciences.

[1] R. Asaro and V. Lubarda, *Mechanics of solids and materials* (Cambridge University Press, 2006).
[2] Y. S. Chen, W. Choi, S. Papanikolaou, and J. P. Sethna, Physical review letters **105**, 105501 (2010).
[3] H. Mughrabi, T. Ungar, W. Kienle, and M. Wilkens, Philosophical magazine A **53**, 793 (1986).

[4] C. Schwink, Scripta metallurgica et materialia **27**, 963 (1992).
[5] P. Hähner, K. Bay, and M. Zaiser, Physical review letters **81**, 2470 (1998).
[6] D. Hughes, Q. Liu, D. Chrzan, and N. Hansen, Acta materialia **45**, 105 (1997).
[7] D. Hughes, D. Chrzan, Q. Liu, and N. Hansen, Physical review letters **81**, 4664 (1998).
[8] E. Laufer and W. Roberts, Philosophical Magazine **14**, 65 (1966).
[9] S. Suresh, *Fatigue of materials* (Cambridge university press, 1998).
[10] H. Mughbrabi, F. u. Ackermann, and K. Herz, "Persistent slipbands in fatigued face-centered and body-centered cubic metals," in *Fatigue Mechanisms* (ASTM International, 1979).
[11] D. Walgraef and E. C. Aifantis, Journal of applied physics **58**, 688 (1985).
[12] D. Kuhlmann-Wilsdorf and C. Laird, Materials Science and Engineering **46**, 209 (1980).
[13] T. Tabata, H. Fujita, M.-A. Hiraoka, and K. Onishi, Philosophical Magazine A **47**, 841 (1983).
[14] N. Goldenfeld, *Lectures on phase transitions and the renormalization group* (Addison-Wesley, Advanced Book Program, Reading, 1992).
[15] D. L. Holt, J. Appl. Phys **41**, 3197 (1970).
[16] D. Walgraef and E. Aifantis, J. Appl. Phys. **58**, 688 (1985).
[17] J. Pontes, D. Walgraef, and E. C. Aifantis, Int. J. Plasti. **22**, 1486 (2006).
[18] J. M. Salazar, R. Fournet, and N. Banal, Acta Metall. Mater. **43**, 1127 (1995).
[19] N. Hansen and D. Kuhlmann-Wilsdorf, Mater. Sci. Eng. **81**, 141 (1986).
[20] J. Kratochvíl and R. Sedlaček, Phys. Rev. B **77**, 134102 (2008).
[21] I. Groma, F. Csikor, and M. Zaiser, Acta Materialia **51**, 1271 (2003).
[22] I. Groma, G. Györgyi, and B. Kocsis, Phys. Rev. Lett. **96**, 165503 (2006).
[23] I. Groma, G. Györgyi, and P. D. Ispánovity, Philos. Mag. **90**, 3679 (2010).
[24] I. Groma, Z. Vandrus, and P. D. Ispánovity, Physical Review Letters **114**, 015503 (2015).
[25] I. Groma, M. Zaiser, and P. D. Ispánovity, Physical Review B **93**, 214110 (2016).
[26] P.-L. Valdenaire, Y. Le Bouar, B. Appolaire, and A. Finel, Physical Review B **93**, 214111 (2016).
[27] W. Prager, Proceedings of the Institution of Mechanical Engineers **169**, 41 (1955).
[28] W. Prager, J. Applied Mechanics **23**, 482 (1956).
[29] N. Fleck, G. Muller, M. Ashby, and J. Hutchinson, Acta Metallurgica et Materialia **42**, 475 (1994).
[30] M. Zaiser, N. Nikitas, T. Hochrainer, and E. Aifantis, Philosophical Magazine **87**, 1283 (2007).
[31] M. M. W. Dogge, R. H. J. Peerlings, and M. G. D. Geers, Advanced Modeling and Simulation in Engineering Sciences **2**, 29 (2015).
[32] R. Wu, D. Tüzes, P. D. Ispánovity, I. Groma, T. Hochrainer, and M. Zaiser, Phys. Rev. B **98**, 054110 (2018).
[33] C. Zhou, C. Reichhardt, C. J. O. Reichhardt, and I. J. Beyerlein, Scientific Reports **5**, 8000 (2015).
[34] M. Zaiser and P. Moretti, J. Stat. Mech. , P08004 (2005).
[35] A. Nicolas, E. E. Ferrero, K. Martens, and J.-L. Barrat, Rev. Mod. Phys. **90**, 045006 (2018).
[36] P. D. Ispánovity, D. Tüzes, P. Szabó, M. Zaiser, and I. Groma, Physical Review B **95**, 054108 (2017).
[37] C. Zhou, C. J. Olson Reichhardt, C. Reichhardt, and I. Beyerlein, Physics Letters A **378**, 1675 (2014).
[38] P. D. Ispánovity, L. Laurson, M. Zaiser, I. Groma, S. Zapperi, and M. J. Alava, Physical review letters **112**, 235501 (2014).
[39] P. D. Ispánovity, I. Groma, G. Györgyi, F. F. Csikor, and D. Weygand, Physical review letters **105**, 085503 (2010).
[40] P. Szabó, P. D. Ispánovity, and I. Groma, Physical Review B **91**, 054106 (2015).
[41] L. Laurson, M.-C. Miguel, and M. J. Alava, Phys. Rev. Lett. **105**, 015501 (2010).
[42] J. Rosti, J. Koivisto, L. Laurson, and M. J. Alava, Phys. Rev. Lett. **105**, 100601 (2010).
[43] S. Papanikolaou, H. Song, and E. Van der Giessen, Journal of the Mechanics and Physics of Solids **102**, 17 (2017).
[44] D. Gómez-García, B. Devincre, and L. P. Kubin, Physical Review Letters **96**, 125503 (2006).
[45] S. Papanikolaou, Y. Cui, and N. Ghoniem, arXiv:1705.06843 [cond-mat] (2017), arXiv: 1705.06843.
[46] B. Devincre, T. Hoc, and L. Kubin, Science **320**, 1745 (2008).
[47] A. El-Azab, Physical Review B **61**, 11956 (2000).
[48] S. Xia and A. El-Azab, Modelling and Simulation in Materials Science and Engineering **23**, 055009 (2015).
[49] Y. S. Chen, W. Choi, S. Papanikolaou, and J. P. Sethna, Physical Review Letters **105**, 105501 (2010).
[50] Y. S. Chen, W. Choi, S. Papanikolaou, M. Bierbaum, and J. P. Sethna, International Journal of Plasticity Microstructure-based Models of Plastic Deformation, **46**, 94 (2013).
[51] T. Hochrainer, S. Sandfeld, M. Zaiser, and P. Gumbsch, Journal of the Mechanics and Physics of Solids **63**, 167 (2014).
[52] T. Hochrainer, Journal of the Mechanics and Physics of Solids **88**, 12 (2016).
[53] R. J. Amodeo and N. M. Ghoniem, Physical Review B **41**, 6958 (1990).
[54] See Supplemental Material at [URL will be inserted by the production group] for details of the applied numerical methods.
[55] J. P. Hirth and J. Lothe, *Theory of Dislocations*, 2nd ed. (John Willey & Sons, New York, 1982).
[56] K. Martens, L. Bocquet, and J.-L. Barrat, Soft Matter **8**, 4197 (2012).
[57] M. Zaiser and S. Sandfeld, Modelling and Simulation in Materials Science and Engineering **22**, 065012 (2014).
[58] O. Kapetanou, D. Weygand, and M. Zaiser, Journal of Statistical Mechanics: Theory and Experiment **2015**, P08009 (2015).
[59] E. Luijten, M. E. Fisher, and A. Z. Panagiotopoulos, Physical Review Letters **88**, 185701 (2002).
[60] M. Zaiser, M.-C. Miguel, and I. Groma, Phys. Rev. B **64**, 224102 (2001).
[61] M. Wilkens, Acta Metall. **17**, 1155 (1969).
[62] R. Morrissey, D. McDowell, and T. Nicholas, International Journal of Fatigue **23(01)**, 55 (2001).
[63] A. Abel and H. Muir, Philosophical Magazine **26**, 489 (1972).
[64] E. Melan, Ing.-Arch. **8**, 116 (1938).
[65] W. Prager, *Introduction to Mechanics of Continua* (Ginn

and Company, Boston, MA, 1961).

[66] K. Shizawa and H. M. Zbib, International Journal of Plasticity **15**, 899 (1999).